

Plasma-Catalytic Methanol Synthesis from CO₂ Hydrogenation over a Supported Cu Cluster Catalyst: Insights into the Reaction Mechanism

Zhaolun Cui, Shengyan Meng, Yanhui Yi,* Amin Jafarzadeh, Shangkun Li, Erik Cornelis Neyts, Yanpeng Hao, Licheng Li, Xiaoxing Zhang,* Xinkui Wang, and Annemie Bogaerts



Cite This: *ACS Catal.* 2022, 12, 1326–1337



Read Online

ACCESS |

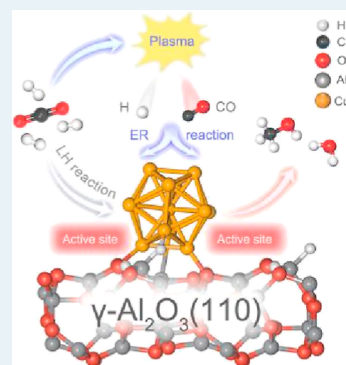
Metrics & More

Article Recommendations

Supporting Information

ABSTRACT: Plasma-catalytic CO₂ hydrogenation for methanol production is gaining increasing interest, but our understanding of its reaction mechanism remains primitive. We present a combined experimental/computational study on plasma-catalytic CO₂ hydrogenation to CH₃OH over a size-selected Cu/γ-Al₂O₃ catalyst. Our experiments demonstrate a synergistic effect between the Cu/γ-Al₂O₃ catalyst and the CO₂/H₂ plasma, achieving a CO₂ conversion of 10% at 4 wt % Cu loading and a CH₃OH selectivity near 50%, further rising to 65% with H₂O addition (for a H₂O/CO₂ ratio of 1). Furthermore, the energy consumption for CH₃OH production was more than 20 times lower than with plasma only. We carried out density functional theory calculations over a Cu₁₃/γ-Al₂O₃ model, which reveal that the interfacial sites of the Cu₁₃ cluster and γ-Al₂O₃ support show a bifunctional effect: they do not only activate the CO₂ molecules but also strongly adsorb key intermediates to promote their hydrogenation further. Reactive plasma species can regulate the catalyst surface reactions via the Eley–Rideal (E–R) mechanism, which accelerates the hydrogenation process and promotes the generation of the key intermediates. H₂O can promote the CH₃OH desorption by competitive adsorption over the Cu₁₃/γ-Al₂O₃ surface. This study provides new insights into CO₂ hydrogenation through plasma catalysis, and it provides inspiration for the conversion of some other small molecules (CH₄, N₂, CO, etc.) by plasma catalysis using supported-metal clusters.

KEYWORDS: nonthermal plasma, catalysis, CO₂, CH₃OH, hydrogenation, Cu₁₃/γ-Al₂O₃



1. INTRODUCTION

Increasing emission of carbon dioxide (CO₂) has resulted in more and more severe greenhouse effects, causing global climate changes. Therefore, extensive efforts have been devoted to CO₂ storage and utilization.^{1,2} Among them, hydrogenation to CH₃OH is a promising way to utilize CO₂.^{3,4} Due to the high activity of a Cu surface, Cu-based catalysts have attracted considerable interest^{5–7} and Cu particles combined with different promoters and supports showed synergistic effects in CO₂ conversion and CH₃OH selectivity.^{8–10} For instance, a Cu/ZnO/Al₂O₃ catalyst is widely used in the chemical industry for CH₃OH synthesis with high CH₃OH selectivity and excellent catalytic stability.^{11–13}

In recent years, supported metal cluster (SMC) catalysts have been gaining great interest as they have advantages such as high activity and high atomic economy, and they show great catalytic potentials.¹⁴ Liu et al. proved that size-selected Cu₄ clusters supported on an Al₂O₃ support have a promising activity for CH₃OH formation at a low CO₂ partial pressure.¹⁵ However, the catalytic mechanism of supported Cu cluster catalysts for CO₂ hydrogenation to CH₃OH remains poorly understood.

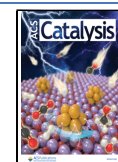
CH₃OH synthesis by CO₂ hydrogenation is favored at low temperature and high pressure as the reaction is exothermic and the number of molecules decreases upon the reaction. However, low-temperature operation suffers from a kinetic limitation in CO₂ activation, in contrast to the thermodynamic limitation of the reaction at high temperatures. In addition, high-pressure operation brings challenges for the reduction of the energy cost. In 2018, Wang et al. demonstrated CO₂ hydrogenation to CH₃OH by nonthermal plasma over Cu/γ-Al₂O₃ catalysts at atmospheric pressure and room temperature.¹⁶ Indeed, highly energetic electrons in the plasma create radicals, which may help to overcome the activation barriers via the Eley–Rideal (E–R) mechanism, as compared to thermal catalysis.^{17–19}

In recent years, plasma-assisted heterogeneous catalysis, simply called “plasma catalysis”, has been applied in C1

Received: October 11, 2021

Revised: December 6, 2021

Published: January 7, 2022



chemistry and has attracted more and more attention.^{20–25} Various “plasma effects” have proven to be beneficial for CO₂ conversion and product yields, which makes plasma catalysis an attractive alternative to thermal catalysis. Therefore, in this paper, we want to explore whether a combination of a Cu cluster catalyst and plasma shows a synergistic effect for CO₂ hydrogenation to CH₃OH.

One of the challenges in plasma catalysis is to gain deeper insight into the synergistic effects between plasma and catalysts. Indeed, the underlying mechanisms in plasma catalysis remain poorly understood. Most of the modeling works focus on macroscopic (chemical kinetics and fluid) models,^{26–28} while simulations at the molecular level are scarce. Nevertheless, the density functional theory (DFT) method is a promising way to provide valuable information on the reaction paths in catalysis.²⁶ DFT studies on thermal catalysis revealed that there are two main paths for CO₂ hydrogenation to CH₃OH, that is, the formate (HCOO) path and the reverse water–gas shift (RWGS) + CO–hydro path (COOH path).^{13,15,29,30} In the HCOO path, the hydrogenation of CO₂ proceeds through H₂COOH* or HCOOH* to H₂CO*, and finally, it forms CH₃OH.^{31,32} In the COOH path, CO₂ is first converted to CO* via COOH* through the RWGS reaction, and then, CO* is converted to CH₃OH by further hydrogenation through HCO*, H₂CO*, and H₂COH* or H₃CO*.

In the present study, we focus on supported Cu cluster catalysts for CO₂ hydrogenation into CH₃OH by plasma catalysis by means of both experiments and DFT calculations. Our experiments demonstrate that γ -Al₂O₃-supported Cu cluster catalysts can significantly improve the production of CH₃OH and reduce the generation of CH₄, with the optimal CH₃OH selectivity reaching 65%. To understand the underlying mechanisms, we performed DFT calculations. We first investigated the reaction pathways for CH₃OH formation via the L–H mechanism. Subsequently, we considered the effects of plasma species participating via the E–R mechanism. Our DFT calculations reveal that the catalytic effects of Cu₁₃/ γ -Al₂O₃ (110) are different from a Cu(111) plane slab or a single Cu cluster studied before due to the metal–support interaction.^{33,34} In the hydrogenation process, the RWGS and formate paths are comparable in the rate-limiting steps for CH₃OH formation via the L–H mechanism. Taking the plasma species into account, the overall hydrogenation barrier is much lower than in the L–H path due to the E–R reactions. The RWGS path is found to be more significant in the case of plasma catalysis since abundant CO molecules are produced and they can promote HCO* generation. Moreover, we found that H₂O facilitates the methanol yield due to its assistance of CH₃OH desorption. This study indicates the potential of plasma catalysis with Cu cluster catalysts for CO₂ hydrogenation to CH₃OH and is in general important for a better understanding of plasma catalysis and its applications, especially with SMC catalysts.

2. MATERIALS AND METHODS

2.1. Preparation of the Cu/ γ -Al₂O₃ Catalyst. The Cu/ γ -Al₂O₃ catalysts with various loadings (1, 2, 3, 4, and 5 wt %) are prepared by the incipient-wetness impregnation method. To remove water and impurities, the γ -Al₂O₃ support is calcined in a muffle furnace at 813 K for 4 h in the air atmosphere. First, the precursor salt, that is, Cu(NO₃)₂·5H₂O, is dissolved in deionized water with varying concentrations

based on the desired loading. Then, the support is added to the solution, and the mixture is stirred at ambient temperature for 30 min, followed by 15 h aging and overnight drying at 393 K in air. After that, the samples are calcined at 673 K for 5 h, and finally, the obtained samples are crushed and sieved to granules in a mesh range of 20–40 (0.85–0.42 mm diameter). Prior to catalytic tests, the samples are reduced by H₂ plasma (40 mL/min H₂, 26 W, 573 K) for 1 h at atmospheric pressure.

2.2. Experimental Steps and Reaction Evaluation. A schematic diagram of the experimental equipment for the plasma-catalytic CO₂/H₂ reaction is shown in the [Supporting Information](#), Figure S1. A coaxial dielectric barrier discharge (DBD) reactor is used to generate CO₂/H₂ plasma. The DBD reactor consists of a pair of coaxial quartz cylinders (inner and outer quartz tubes) in which a stainless-steel (2 mm outer diameter) electrode is placed in the center, and circulating water is pumped into the space between the inner and outer cylinder, acting as a ground electrode. The discharge length is 60 mm, and the discharge gap is fully packed by catalyst granules (0.85–0.42 mm diameter). CO₂ (18 mL/min) and H₂ (54 mL/min) are monitored by calibrated mass flow controllers and mixed homogeneously with water vapor before passing through the plasma reactor. Indeed, water vapor is added (up to H₂O/CO₂ molar ratios of 1) to investigate its effect on the CO₂ conversion and CH₃OH selectivity. The water vapor is generated by a steam generator (FD-HG from Furande Equipment Co., Ltd.). The discharge frequency is fixed at 9.5 kHz, and the applied power is maintained at around 26 W. The liquid product is collected by a cold trap at the exhaust of the DBD reactor. A gas chromatograph (Tianmei 7890 II equipped with a thermal conductivity detector and a TDX-01 column) is used to analyze the composition of the exhaust gases. The liquid products are quantitatively analyzed by another gas chromatograph (Shimadzu GC-2014C equipped with a flame ionization detector and a PEG-20M column). The variation of the gas volume is measured by a soap-film flow meter. The exhaust gas is analyzed online by a mass spectrometer (Pfeiffer Vacuum GSD301) with the Faraday detection mode. The reaction temperature in the discharge area is close to the circulating water temperature (ca. 60 °C), while the temperature near the high-voltage electrode may be slightly higher than 60 °C.¹⁶

To evaluate the reaction performance, the CO₂ conversion is calculated by eq 1

$$X_{\text{CO}_2} = \frac{\text{CO}_{2[\text{in}]} - \text{CO}_{2[\text{out}]}}{\text{CO}_{2[\text{in}]}} \times 100\% \quad (1)$$

In the tail gas, only CO and CH₄ are detected by the gas chromatograph. The selectivity of CO and CH₄ is calculated by eqs 2 and 3, respectively

$$S_{\text{CO}} = \frac{\text{CO}_{[\text{out}]}}{\text{CO}_{2[\text{in}]} - \text{CO}_{2[\text{out}]}} \times 100\% \quad (2)$$

$$S_{\text{CH}_4} = \frac{\text{CH}_{4[\text{out}]}}{\text{CO}_{2[\text{in}]} - \text{CO}_{2[\text{out}]}} \times 100\% \quad (3)$$

In the collected liquid, only one single product, CH₃OH, is detected by our gas chromatograph. Thus, the selectivity of CH₃OH is calculated by eq 4

$$S_{\text{CH}_3\text{OH}} = 1 - S_{\text{CO}} - S_{\text{CH}_4} \quad (4)$$

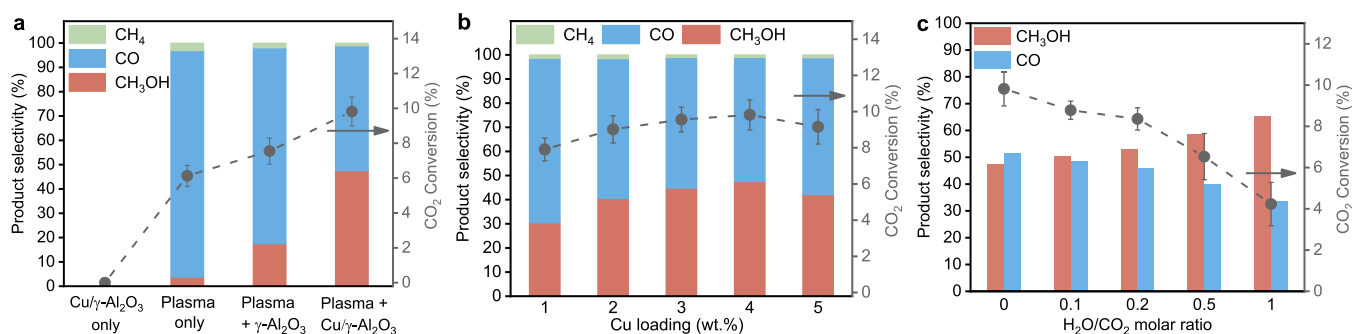


Figure 1. Measured product selectivity and CO₂ conversion for CO₂ hydrogenation over the Cu/γ-Al₂O₃ catalyst: (a) for catalysis-only [CO₂/H₂ = 1:3, weight-hourly space velocity (WHSV) = 2400 mL/g/h], plasma-only, and plasma catalysis with γ-Al₂O₃ and 4% Cu/γ-Al₂O₃ catalysts (CO₂/H₂ = 1:3, WHSV = 2400 mL/g/h, 26 W input power). (b) For plasma catalysis with different Cu loadings (CO₂/H₂ = 1:3, WHSV = 2400 mL/g/h, 26 W input power). (c) For plasma catalysis with different H₂O/CO₂ molar ratios (total CO₂/H₂ flow rate = 72 mL/min with 1:3 ratio).

The energy consumption for CH₃OH generation is calculated by eq 5

$$\text{energy consumption (kJ/mmol)} = \frac{\text{discharge power (J/s)}}{\text{rate of CH}_3\text{OH produced (mol/s)}} \times 10^{-6} \quad (5)$$

where the factor 10^{−6} accounts for the conversion of J/mol into kJ/mmol.

2.3. Catalyst Characterization. The crystal structure of the catalyst is determined by using Cu Kα radiation (40 kV, 50 mA) on a Rigaku D/Max2400 powder X-ray diffractometer, and the sample is scanned from 10 to 80° at a step of 10°/min. High-angle annular dark-field scanning transmission electron microscopy (HAADF-STEM) and elementary mapping are performed on a JEM-ARM200F electron microscope at 200 kV. The specific surface area, pore volume, and pore size of the catalysts are measured by N₂ physisorption (Micromeritics ASAP 3020). Prior to the measurements, the catalysts are vacuum-treated at 623 K for 5 h to remove impurities adsorbed in the catalyst pores. The reduction properties of the catalysts are determined using H₂ temperature-programmed reduction (H₂-TPR) on a Quantachrome ChemBET Pulsar TPR apparatus. The samples (0.15 g) are purged for 1 h at 723 K under a He atmosphere. After cooling to room temperature, the samples are heated from room temperature to 773 K in an Ar–H₂ (120 mL/min, 10% H₂) atmosphere at a rate of 10 K/min, and the signal of H₂ consumption is collected. X-ray photoelectron spectroscopy (XPS) is performed on an ESCALAB250 instrument (ThermoVG, USA) with an Al Kα X-ray source.

2.4. Optical Emission Spectrometry. A Princeton Instruments ICCD spectrometer (SP 2758) with a 300 g/mm grating is used to in situ diagnose the CO₂/H₂ plasma (200–1200 nm). The slit width of the spectrometer is fixed at 20 μm, and the exposure time is fixed at 2 s.

2.5. Computational Details. All DFT calculations are carried out in the CP2K 7.0 package.³⁵ The Gaussian and plane-wave method in the quickstep module is applied to calculate the energies and forces.^{36,37} The molecularly optimized (MOLOPT) double-ζ valence plus polarization (m-DZVP) basis set is used, combined with a 600 Ry cutoff set for the plane-wave calculation. Goedecker–Teter–Hutter pseudopotentials are applied to treat the inner-shell electrons.^{38,39} The Perdew–Burke–Ernzerhof functional in the generalized gradient approximation is chosen to describe

the exchange correlation energy.⁴⁰ For dispersion correction, Grimme's D3 method with Becke–Johnson damping is applied.⁴¹ The Broyden–Fletcher–Goldfarb–Shanno scheme is used for the geometry optimization.⁴²

The *k*-point sampling is limited to the Γ point only. The atomic charge analysis is calculated by the Bader scheme.⁴³ The transition-state (TS) calculations are carried out by the climbing image nudged elastic band method.⁴⁴ Vibrational analysis is carried out for the TS validation to ensure that there is only one imaginary frequency in each TS structure.

The widely used γ-Al₂O₃(110) surface is chosen to be the support slab.⁴⁵ It is modeled as a 2 × 2 supercell and contains 4 layers and 160 atoms. This structure has been used as a support for Ni cluster adsorption to activate CO₂ molecules.⁴⁶ The bottom two layers are fixed during the whole calculation. The simulation cell dimensions are 16.1439 × 16.7874 × 40.0000 Å³ with a periodic boundary along the XYZ directions.

As for the γ-Al₂O₃ surface termination, the “dry” γ-Al₂O₃(110) surface is not very stable and often hydrated (preadsorbed H and OH).⁴⁷ Besides, in plasma catalysis with H₂ gas being involved, the plasma offers plenty of H atoms to adsorb on the catalyst surface, known as the “net effect”.⁴⁸ Therefore, in this model, we placed eight H atoms instead of four H and four OH on the γ-Al₂O₃(110) surface, and the adsorption sites for H atoms are set the same as the H and OH sites for a “hydrated” γ-Al₂O₃(110) surface.^{47,49} After this treatment, the H-coverage ratio for the γ-Al₂O₃ surface is 0.125 ML. Further investigation for the net effect and the H-coverages on the CO₂ hydrogenation process is out of scope and is not discussed in this paper.

The adsorption energy (*E*_{ad}) of the Cu₁₃ cluster on the γ-Al₂O₃ surface is calculated by eq 6

$$E_{\text{ad}} = E_{\text{slab+cluster}} - E_{\text{slab}} - E_{\text{cluster}} \quad (6)$$

where *E*_{slab} and *E*_{cluster} are the total energies of the γ-Al₂O₃ slab and Cu₁₃ cluster, respectively, and *E*_{slab+cluster} is the total energy of the Cu₁₃ cluster adsorbed on the γ-Al₂O₃ system.

The adsorption energy of gas molecules on the Cu₁₃/γ-Al₂O₃ surface is calculated by eq 7

$$E_{\text{ad}} = E_{\text{gas+complex}} - E_{\text{gas}} - E_{\text{complex}} \quad (7)$$

where *E*_{gas} and *E*_{complex} are the energies of gas molecules and the Cu₁₃/γ-Al₂O₃ system, respectively, and *E*_{gas+complex} is the total energy of the gas molecules adsorbed on the Cu₁₃/γ-Al₂O₃ system. The binding energy (BE) of the intermediates on the Cu₁₃/γ-Al₂O₃ interface is also calculated by eq 7, where

E_{gas} is replaced by the energy of the intermediates, such as COOH, HCOO, and so on.

3. RESULTS AND DISCUSSION

3.1. Measured Product Selectivity, CO₂ Conversion, and Energy Consumption. Figure 1 shows the CO₂ hydrogenation results over a Cu/ γ -Al₂O₃ catalyst. As illustrated in Figure 1a, in the absence of plasma, the CO₂ conversion is zero, indicating that CO₂ cannot be converted at room temperature and atmospheric pressure without the assistance of plasma. In the case of plasma only, the CO₂ conversion reaches 6.1% but with only 3.7% CH₃OH selectivity. After packing the CO₂/H₂ plasma with γ -Al₂O₃, the CO₂ conversion and CH₃OH selectivity increase to 7.6 and 17.4%, respectively, while adding the Cu/ γ -Al₂O₃ catalyst (4 wt % loading) yields a further increase in the performance: the CO₂ conversion and CH₃OH selectivity increase to 9.8 and 47.5%, respectively. These results demonstrate that the Cu/ γ -Al₂O₃ catalyst has a synergistic effect with plasma, resulting in a high activity toward CO₂ conversion and CH₃OH synthesis.

Figure 1b shows the performance of the Cu/ γ -Al₂O₃ catalysts with various loadings. The CO₂ conversion and CH₃OH selectivity first increase and then decrease upon increasing Cu loading, and the optimum loading is 4 wt % under these experimental conditions.

In addition, we investigated the influence of H₂O on the CH₃OH synthesis, as shown in Figure 1c. Upon increasing the H₂O/CO₂ molar ratio from 0:1 to 1:1, the CH₃OH selectivity increases from 47.5 to 65.2%, while the CO selectivity decreases from 51.4 to 33.6%. The CO₂ conversion, on the other hand, drops upon H₂O addition, which is attributed to the competitive adsorption on the active sites, as will be shown by our DFT calculations. Furthermore, Figure S2 shows that a high content of H₂O reduces the discharge voltage and current. It is clear that when the H₂O/CO₂ ratio rises from 1.0 to 1.5, the discharge voltage and the current are more significantly reduced. This could also be a possible reason for the lower CO₂ conversion presented in Figure 1c.

To understand the role of H₂O in improving the CH₃OH selectivity, we analyzed the exhaust gas during the reaction by online mass spectrometry. As shown in Figure S3, after switching on the plasma, the signal intensity of *CH₃O increases, which represents the production of CH₃OH. Interestingly, a sharp increase of the *CH₃O signal is observed after each H₂O injection, indicating that more CH₃OH is produced after adding H₂O to the feedstock. This experimental result can be explained by promoting the function of H₂O in CH₃OH desorption, as revealed by our DFT calculations (see Section 3.7 below), as well as in literature studies.^{50–52}

Note that we also performed experiments in a CO₂/H₂O plasma (both in the absence and presence of the Cu/ γ -Al₂O₃ catalyst). Indeed, H₂O vapor could be an interesting source of H, as also demonstrated by Gorbanev et al. for another application, that is, catalyst-free and H₂-free NH₃ synthesis from N₂/H₂O mixtures.⁵³ However, in our experiments, the measured CO₂ conversion in the CO₂/H₂O plasma was nearly zero, and no CH₃OH was detected in the collected liquid. This corresponds well with an earlier paper by Snoeckx et al., where the drop in CO₂ conversion upon the addition of H₂O vapor, as well as the absence of CH₃OH formation, was explained by chemical kinetic modeling, that is, more specifically due to the recombination reaction of CO with OH radicals, forming CO₂ again.⁵⁴ In addition, Zhao et al. obtained CH₃OH and

CH₃CH₂OH using a CO₂/H₂O plasma, but the yields were only in the micromolar level.⁵⁵

The energy consumption is also a key indicator for plasma catalysis. We present the energy consumption of CH₃OH generation under different conditions in Figure 2. It is clear

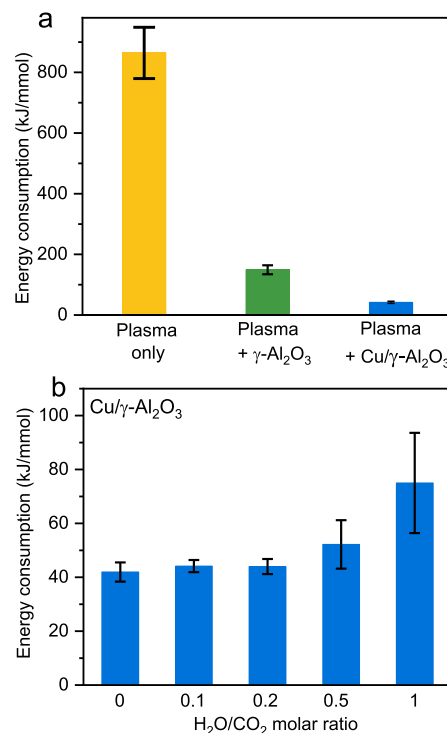


Figure 2. Energy consumption for CH₃OH generation: (a) for plasma-only, plasma + γ -Al₂O₃, and plasma + Cu/ γ -Al₂O₃ and (b) for plasma catalysis with different H₂O/CO₂ molar ratios.

that the energy efficiency is significantly improved by combining the plasma and the Cu/ γ -Al₂O₃ catalyst as the energy consumption drops from 855.9 kJ/mmol in the plasma-only system to 147.7 kJ/mmol in the plasma + γ -Al₂O₃ system, and it eventually drops to 41.6 kJ/mmol in the plasma + Cu/ γ -Al₂O₃ system, as shown in Figure 2a. This reduction in energy consumption by more than a factor of 20 indicates the key role of the active metal (Cu cluster) for efficiently producing CH₃OH. On the other hand, in Figure 2b, we show that increasing the H₂O concentration enlarges the energy consumption, indicating that its negative impact on CO₂ conversion is stronger than its promotional effect on CH₃OH generation.

Furthermore, under all conditions, the CH₄ selectivity remains at a low level (<2%), which is in line with the literature, showing a hindering effect of Cu-based catalysts on CH₄ yields.¹⁵ This will be explained in our DFT results due to the high activation barriers for CH₄ production (see Section 3.5).

Table S1 in the Supporting Information compares our results (for plasma catalysis) with some representative results from the literature for conventional thermal catalysis. It is clear that our plasma catalysis experiments exhibit a similar degree of CO₂ conversion as conventional thermal catalysis. The selectivity toward CH₃OH in our plasma catalysis experiments is a little lower than in the conventional thermal catalysis, which is attributed to the high reactivity of the CO₂/H₂

plasma, leading also to the production of CO through the RWGS reaction. With regard to the reaction conditions, conventional thermal catalysis generally needs to be operated at higher temperature (180–300 °C) and higher pressure (0.5–36 MPa), while plasma catalysis can be operated at ambient temperature and atmospheric pressure, which is the main advantage compared to the conventional thermal catalysis. Finally, the energy consumption is also presented in Table S1, but since the data of conventional thermal catalysis are expressed in different units, we could not compare the energy consumption between plasma catalysis and thermal catalysis.

3.2. In Situ OES to Detect the Important Plasma Species in the CO₂/H₂ Plasma. We applied in situ optical emission spectroscopy (OES) to detect the important species in the CO₂/H₂ plasma, as presented in Figure 3. The CO₂/H₂

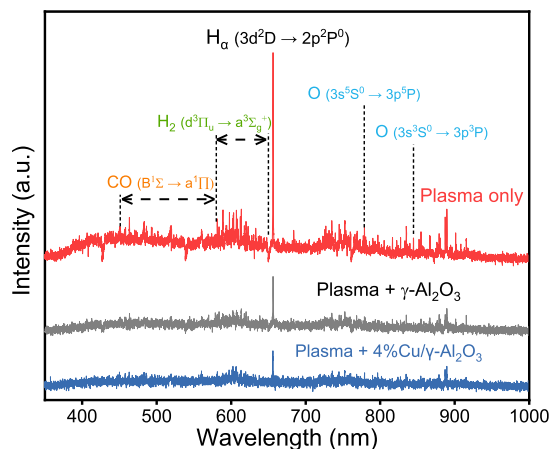


Figure 3. OES results for different plasma catalysis conditions.

plasma in the absence of a catalyst or support shows the highest signal intensity, including several spectral lines and two

spectral bands: the H_α line⁵⁶ (656.3 nm, 3d²D → 2p²P⁰), two O atomic spectral lines^{57,58} (777.5 nm, 3s⁵S⁰ → 3p⁵P; 844.7 nm, 3s³S⁰ → 3p³P), a H₂ band (580–650 nm, d³Π_u → a³Σ_g⁺), and a CO band (450–580 nm, B¹Σ → A¹Π).⁵⁹ This indicates that H atoms and CO molecules are abundantly produced in the plasma region.

The signal intensity was obviously reduced after packing the support, which may be caused by the shielding effect.⁶⁰ Interestingly, the signal intensity was further reduced after packing with the Cu/γ-Al₂O₃ catalyst. To verify if this was caused by optical interference from the packed catalysts, we used UV–vis spectroscopy to study the light absorption properties of the Cu/γ-Al₂O₃ catalyst. We can see from Figure S4 in the Supporting Information that the Cu/γ-Al₂O₃ catalyst shows an obvious absorption peak for UV-light (200–400 nm) but a much lower absorption intensity for visible light (400–800 nm). Because all the lines and bands of interest are located in the wavelength range of visible light, it is reasonable to believe that the reduction of the OES intensity is caused not only by optical interference from the packed catalysts but also by the ability of the active sites to adsorb the reactive species. The reactive CO and H species could promote the CH₃OH production via E–R reactions over the catalyst surface (see Section 3.6 below). Besides, changes in the relative strength of the peaks in these three OES systems correspond well with the product selectivity in Figure 1a, where the CO selectivity exceeds 90% in the plasma-only system, while the CH₃OH selectivity significantly increases when the Cu/γ-Al₂O₃ catalyst is packed in the reactor.

According to Figure S5, the OES intensity decreases with increasing H₂O/CO₂ molar ratio, which is probably caused by the ionization of H₂O. Besides, as could be deduced from Figure S2, the discharge performance is reduced by adding H₂O, especially the intensity of the filaments. This may indicate that at higher H₂O content, more energy is consumed by the ionization of H₂O, and less energy is consumed by CO₂

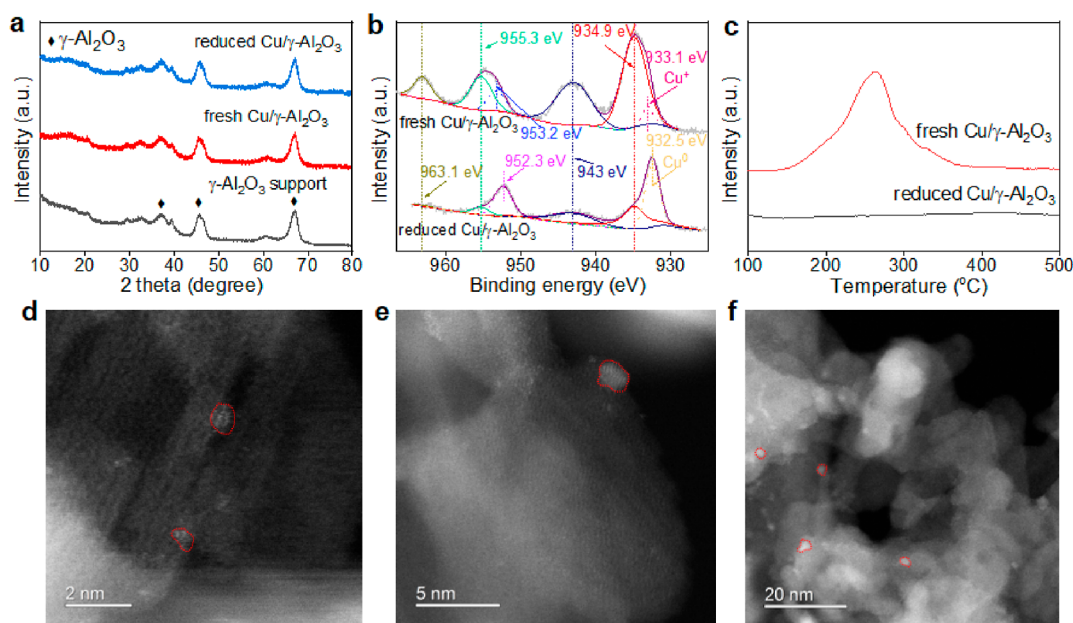


Figure 4. Characterization of the Cu/γ-Al₂O₃ catalyst: (a) XRD patterns; (b) Cu 2p XPS spectra; (c) H₂-TPR profiles; (d–f) HAADF-STEM images.

and H₂. Hence, this process negatively impacts the CH₃OH production, resulting in a higher energy consumption.

3.3. Catalyst Characterization. We characterize the Cu/ γ -Al₂O₃ catalyst (with 4 wt % loading) by X-ray diffraction (XRD), XPS, H₂-TPR, and HAADF-STEM and present them in Figure 4. More information about the catalysts, that is, N₂ physisorption data (Table S2) and elementary mapping results (Figure S6), can be found in the Supporting Information. Figure 4a shows the XRD results. The diffraction peaks are all attributed to γ -Al₂O₃, and no diffraction peaks related to the Cu species are observed for the Cu-based catalysts, indicating that Cu is highly dispersed on γ -Al₂O₃. Figure 4b shows the XPS results. For the fresh sample, two peaks at 934.9 and 955.3 eV are observed, and they are attributed to Cu 2p_{3/2} and Cu 2p_{1/2} of the Cu²⁺ species, respectively. In addition, the presence of Cu²⁺ is confirmed by the appearance of oscillating satellite peaks at 943 and 963.1 eV.⁶¹ For the reduced samples, the apparent weakening of the signal intensity at 934.9 and 955.3 eV, as well as the two satellite peaks, demonstrates the disappearance of the Cu²⁺ species, which is caused by the H₂ plasma reduction.⁶² The peaks of the Cu²⁺ species are observed only with low intensity, which is attributed to the fact that the catalyst is susceptible to being oxidized by air (during the transfer of the sample from the plasma reactor to the XPS instrument) to produce CuO species on the sample surface. Even so, two peaks (932.5 and 952.3 eV) assigned to the Cu⁰ species are observed with a much higher intensity than those of the Cu²⁺ species, which means that the Cu⁰ species are dominant in the reduced sample. This observation is consistent with the H₂-TPR results (Figure 4c), where no distinctive peaks are seen for the reduced catalyst, suggesting that Cu^{m+} are all reduced to Cu⁰ at 573 K.

Figure 4d–f shows the HAADF-STEM images of the 4 wt % Cu/ γ -Al₂O₃ samples. Clearly, Cu is highly dispersed on the γ -Al₂O₃ support, with the particle size in the range of 0.8–2 nm. In our DFT calculations, we consider a Cu₁₃ cluster on γ -Al₂O₃, which roughly corresponds to the same particle size as in our experiments. Indeed, it is extremely challenging to synthesize a Cu/ γ -Al₂O₃ catalyst with pure Cu₁₃ clusters, but the DFT results should be able to provide more insights into the underlying mechanisms to explain the experimental results.

The spent Cu/ γ -Al₂O₃ catalyst after 3 h plasma reaction has been characterized by XRD, H₂-TPR, and XPS (Figure S7), which shows the coexistence of the Cu⁰, Cu⁺, and Cu²⁺ species. Hence, the Cu species cannot remain in the Cu⁰ valence state during the CO₂/H₂ plasma reaction since O atoms from CO₂ dissociation will oxidize Cu⁰ to produce Cu₂O and CuO. On the other hand, H species from H₂ dissociation play the role of a reducing agent. Therefore, the CO₂/H₂ plasma reaction comprises a dynamic reduction–oxidation process, yielding a dynamic reduction–oxidation of the Cu species (Cu⁰, Cu⁺, and Cu²⁺).

In the following sections, we will study the CO₂ hydrogenation to CH₃OH over the Cu₁₃/ γ -Al₂O₃ surface by DFT calculations to obtain more insights into the underlying mechanisms. First, we will present the activation of CO₂ over the Cu₁₃/ γ -Al₂O₃ surface. Next, we will analyze the hydrogenation pathways of CO₂ to CH₃OH and CH₄ via the L–H mechanism. Finally, we will present the E–R reactions caused by the reactive plasma species and analyze the promotion effect of H₂O molecules on CH₃OH desorption.

3.4. Cu₁₃ Supported on γ -Al₂O₃(110) and CO₂ Adsorption Site Selection. The Cu₁₃ icosahedron cluster

is a common and stable structure, which has been used to represent Cu nanocluster structures in previous DFT studies.⁴⁹ In this work, the Cu₁₃/ γ -Al₂O₃(110) model is chosen to represent Cu clusters supported by a γ -Al₂O₃ slab, as shown in Figure S9. The Cu₁₃ cluster is first optimized in the gas phase and subsequently allowed to adsorb on the γ -Al₂O₃ substrate, with the Cu atoms binding with the surface O and Al atoms. The adsorption energy E_{ad} is –4.35 eV, which is weaker than the adsorption on a typical hydrated γ -Al₂O₃ surface (–6.13 eV).⁴⁹ This may be caused by the difference in the preadsorbed species on the γ -Al₂O₃ surface.

Before the hydrogenation calculation, we first tested the potential adsorption sites on the Cu₁₃/ γ -Al₂O₃(110) surface. According to SMC studies, the interface of the metal cluster and the support are most likely to be the active sites.^{14,45,63}

Therefore, five typical sites are selected, four of them are interfacial sites around the Cu₁₃ cluster, and one site is on the top of the cluster, as shown in Figure S10. The adsorption energies of two reactants (CO₂ and H₂) and two products (CH₃OH and H₂O) are calculated and are summarized in Table S3. It is clear that site number 3 at the cluster–slab interface is the most stable site for all four molecules (CO₂, H₂, CH₃OH, and H₂O). Therefore, site number 3 is chosen as the active site for further calculations, and the most stable configurations of the four molecules are shown in Figure S11.

As shown in Figure S12a, after the adsorption, the CO₂ molecule at the Cu₁₃/ γ -Al₂O₃ interface binds with the Cu atoms and with the slab Al atom, with an O–C–O angle bending from 180 to 121.08°. The two C–O bonds are elongated from 1.18 to 1.29 Å. According to the Bader charge analysis and the charge density difference in Figure S12b, the adsorbed CO₂ molecule gains 1.24 *lel*, where the C atom gains 1.64 *lel*, and the O1 and O2 atoms lose 0.31 *lel* and 0.09 *lel*, respectively. The above results indicate that when the CO₂ molecule is adsorbed, the Cu₁₃/ γ -Al₂O₃ catalyst acts as an electron donor to transfer electrons to the C atom, while it acts as an electron acceptor to take electrons from the O atoms, leading to a weakening of the C–O bonds. In contrast, we found that the adsorption and activation of CO₂ molecules on the Cu₁₃ cluster surface are a bit weaker. In Figure S12c, the O–C–O angle bends from 180 to 134.48° and the two C–O bonds stretch from 1.18 to 1.28 and 1.22 Å, respectively. This result agrees well with former DFT results,⁶³ and the adsorbed CO₂ coordinated in the metal–support interface becomes more active for further reactions. Among all the calculated sites, number 3 interfacial site shows a better effect for CO₂ activation.

In addition, we found that the H₂ adsorbed at the Cu₁₃/ γ -Al₂O₃ interface is decomposed to two H* without an obvious barrier, as shown in Figure S11b, which agrees with previous DFT results.³¹ Moreover, we tested the H₂ decomposition on the Cu₁₃ surface and it has a very small barrier of 0.44 eV. Thus, the H₂ decomposition will not be involved in detail in the subsequent hydrogenation reactions.

3.5. CH₃OH Synthesis at the Interface of Cu₁₃/ γ -Al₂O₃ via the L–H Mechanism. The main reaction pathways for CH₃OH formation and one additional pathway for CH₄ formation are shown in Figure 5. All the elementary reactions are first calculated via the L–H mechanism. The rate-limiting step of the formate path is HCOOH formation with a barrier of 1.32 eV, which is smaller than the rate-limiting step of the RWGS path, that is, COOH* formation (“*” means the adsorbed species), with a barrier of 1.51 eV. The results of the

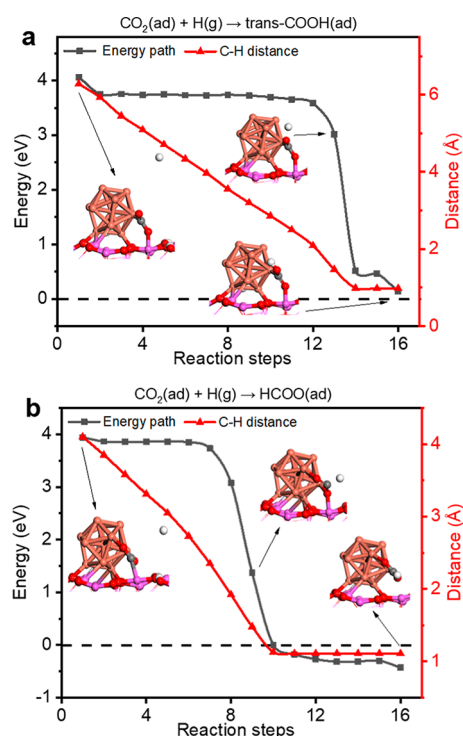


Figure 5. Formation of COOH and HCOO via the E-R mechanism. (a) COOH; (b) HCOO.

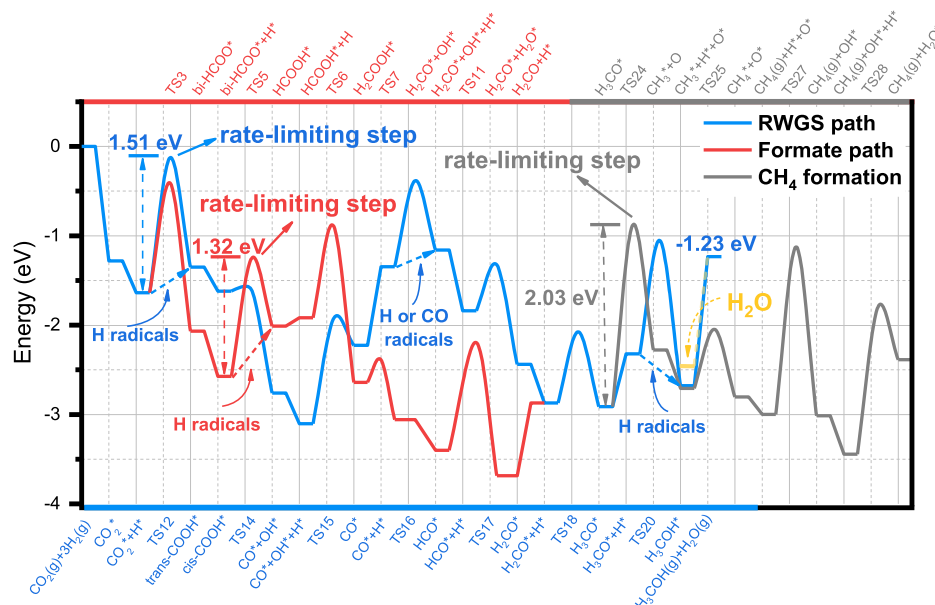
rate-limiting steps in different paths of Cu-based catalysts similarly appeared in previous studies.^{15,32,64} The BE of important intermediates and the reaction barrier and heat of elementary reactions are listed in Tables S4 and S5, respectively. The intermediates in CH₃OH synthesis can be stably adsorbed at the Cu₁₃/γ-Al₂O₃ interfacial site, resulting in an energetically lower reaction pathway.

In the formate path, HCOO* is first generated by CO₂ hydrogenation. Subsequently, HCOO* is hydrogenated to

formic acid (HCOOH*) with a further hydrogenation of HCOOH* to H₂COOH*. Afterward, H₂COOH* is decomposed to H₂CO* and OH* with the breaking of the C–OH bond. Further hydrogenation of H₂CO* leads to the formation of CH₃OH via H₂COH* or H₃CO*. In Scheme S1, we compare the energy barrier of three paths from HCOO* to H₂CO*. The HCOOH* path exhibits the lowest barrier of 1.32 eV, while the other two paths via H₂COO* show barriers of 2.11 and 1.51 eV, respectively. This indicates that the HCOOH* path is more favored than the two H₂COO* paths over the Cu₁₃/γ-Al₂O₃ surface, and a similar distribution of the barriers is also found on the Cu(111) surface.³¹ Moreover, both in our model and on the Cu(111) surface, the BE of HCOOH* (−2.01 eV) is lower than that of H₂COO* (−2.34 eV), which shows a similar catalytic effect of Cu atoms either as a cluster or being a bulk.

Besides, we calculated the CH₃OH formation from H₂CO* hydrogenation via H₂COH* or H₃CO* intermediates, as shown in Scheme S2. These two paths have very similar barriers, that is, 1.27 eV in the H₂COH path and 1.25 eV in the H₃CO path. The barrier of the H₃CO* path is slightly lower than that of the H₂COH* path, and its energy curve lies lower than that for the H₂COH* path. Besides, the BE of CH₃O* (−4.52 eV) is much higher than that of H₂COH* (−2.83 eV), resulting in a higher stability of CH₃O*. Previous studies have shown that the higher stability and abundance of H₃CO* may counteract the higher activation barrier and make the H₃CO* path dominant.^{31,65,66} Therefore, we take the H₃CO* path as the main path, and this is summarized in Scheme 1. In this pathway, the elementary steps of HCOO* to HCOOH* and H₃CO* to CH₃OH show the highest reaction barriers, consistent with the result in a Cu–ZnO system, where the Cu–ZnO interface also acts as an active site.¹³ This may indicate that the combination of the metal–oxide form of Cu-based catalysts provides active sites at the interface over the nanoparticle/slab structure, which shows a multiple catalytic effect on both the activation and the hydrogenation of CO₂.

Scheme 1. Reaction Pathways of CO₂ Hydrogenation to CH₃OH and CH₄; Species Adsorbed at the Active Sites Are Labeled as “*”; to Make the Figure More Readable, H₂ Decomposition and H₂O Desorption Are Omitted from the Pathways



In the COOH path, the barrier for CO₂ hydrogenation to COOH* is 1.51 eV, which is higher than that for the HCOO* formation (1.23 eV), and it makes this reaction become the rate-limiting step for this path. Afterward, COOH* can easily decompose to CO* and OH* at the Cu₁₃/γ-Al₂O₃ interface without an obvious barrier, which is similar to the results on a single Cu₂₉ cluster or on a Cu(111) slab.^{32,33} Subsequently, CO* is gradually hydrogenated to H₂CO* via HCO*. As shown in Table S3, the BE of CO* at the interfacial site is −1.98 eV, corresponding to a chemical adsorption with strong surface interactions. This promotes further hydrogenation rather than a desorption process.⁶⁷ Overall, the RWGS path lies higher than the formate path in energy distribution, which means that the RWGS path is more significant at high temperature. In plasma catalysis, the reactor is maintained at a relatively low temperature (around 400 K). Therefore, if not considering the plasma effect, the formate path is likely to be predominant due to its lower rate-limiting step.

Apart from the RWGS path, CO* may also be generated by CO₂* decomposition. However, one C–O bond-breaking requires 2.08 eV (Table S4), that is, much higher than the hydrogenation reactions, which indicates that direct decomposition of CO₂ to CO is difficult on a Cu₁₃/γ-Al₂O₃ surface.

Moreover, we calculated the path of CH₄ formation. This path begins with the decomposition of H₃CO*. As shown in Scheme 1, the cleavage of the C–O bond for H₃CO* species needs to overcome a high barrier (2.03 eV), much higher than in H₃CO* hydrogenation, which is in agreement with a previous DFT study.¹⁵ Although the hydrogenation of CH₃* to CH₄ (g) has a low barrier of 0.66 eV, the following hydrogenation steps for the decomposition of O* to OH* and further to H₂O* also have high barriers (1.87 and 1.64 eV). Therefore, the DFT results indicate that CH₄ formation via the above path has much higher barriers than CH₃OH production, which can explain the much lower yield of CH₄ in the experiment.

3.6. Effect of Plasma Species via the E–R Mechanism.

Previous studies have demonstrated that plasma species can participate in surface hydrogenation reactions via the E–R mechanism.^{68,69} 1D fluid plasma chemistry simulations showed that in the CO₂/H₂ plasma, H and CO are the two most abundant species.⁷⁰ Therefore, we considered these two plasma species for studying the plasma effects via the E–R reactions. Along the two reaction paths, the initial step for CO₂ hydrogenation, the rate-limiting steps, and the final CH₃OH formation reaction are calculated with the participating H radicals. Besides, the CO molecules are considered to be bonded with H* to form the HCO* species as an alternative way for the RWGS path. Compared with the L–H reactions, the activation barriers are obviously reduced in the E–R reactions when the plasma species are involved. For instance, it can be seen in Figure 5 that *trans*-COOH* and HCOO* are formed when CO₂* binds with gas-phase H radicals without a barrier. At the very start, the energy of the whole system is much higher than in the L–H reaction, which is attributed to the reactive H species generated in the plasma.⁶⁰ The gas-phase H atom moves to the Cu₁₃/γ-Al₂O₃ interface and binds with CO₂, which leads to a sharp decrease of the system energy when the O–H distance approaches about 2 Å. This barrierless E–R reaction indicates that the plasma-generated H atoms may accelerate the CO₂ hydrogenation by changing the reaction mechanism. Similar results are observed in the formation of HCOOH and CH₃OH. In Figure S13,

HCOOH* is generated from HCOO* hydrogenation with H radicals, with the barrier reducing from 1.32 to 0.17 eV, which indicates that the HCOOH formation may no longer be the rate-limiting step in the formate path. In Figure S14, H₃CO* hydrogenation with H radicals to form CH₃OH has a barrier of 0.15 eV, much lower than the barrier of the L–H reaction, that is, 1.25 eV.

Besides, HCO* can be generated when the gas-phase CO species bind with H* or the gas-phase H atoms bind with CO* via two barrierless E–R reactions, as shown in Figures S15 and S16. These two barrierless reactions prove that the CO and H species generated in the plasma are highly reactive and can facilitate HCO* formation. It is known that HCO is an important intermediate and its stability on the catalyst surface is also identified as a key factor affecting the whole RWGS path.³³ In addition, the binding strength of key intermediates over metal-oxide catalysts may also determine the reaction types and selectivity of CO₂ hydrogenation. In our calculations, HCO* can be generated in both L–H and E–R reactions and can be stably adsorbed at the interfacial site.⁶⁷ Besides, our OES results prove that CO and H are abundantly produced in the plasma and can be effectively adsorbed on the catalyst surface to take part in further reactions. Therefore, in plasma catalysis, the RWGS path may become more significant as the HCO* species generated via the E–R reactions may provide an alternative way for CH₃OH* formation with lower barriers.

In thermal catalysis, intermediates such as HCOO may also be produced via the E–R mechanism. Compared to reactions involving the radicals, the reduction in activation barriers is limited and the barriers cannot be eliminated.^{71,72} Overall, the plasma effect can influence the CO₂ hydrogenation via the E–R reactions. The participation of plasma species significantly reduces or even eliminates the energy barriers and in the meantime provide key intermediates for the elementary reactions, resulting in a high CH₃OH selectivity and yield at such low temperatures (ct. 60 °C) and at atmospheric pressure.

3.7. Role of H₂O in CH₃OH Desorption. As mentioned above, the plasma effect can accelerate the hydrogenation process, but it may not necessarily promote CH₃OH desorption. In previous studies, the H₂O molecule has been demonstrated to be an effective promoter for CH₃OH* generation and desorption.^{32,73,74} Therefore, we calculated the CH₃OH *E*_{ad} and configurations in the presence and absence of preadsorbed H₂O, as shown in Table 1 and Figure S17, respectively. In the absence of H₂O, CH₃OH* is stably adsorbed at the Cu₁₃/γ-Al₂O₃ interface with an adsorption energy *E*_{ad} of −1.45 eV (Figure S11a). When H₂O is preadsorbed, the *E*_{ad} of CH₃OH* reduces. In Figure S17d, one H₂O molecule can be coadsorbed with CH₃OH at the Cu₁₃/γ-Al₂O₃ site and the *E*_{ad} of CH₃OH* decreases to −1.23 eV. In Figure S17f, CH₃OH adsorbed at the nearby γ-Al₂O₃ slab has an *E*_{ad} of −1.25 eV, which is more stable than at the interfacial site. When two H₂O molecules are preadsorbed at the interfacial site, the *E*_{ad} of CH₃OH* reduces to −1.17 eV (Figure S17g), which is also weaker than at the γ-Al₂O₃ slab site (−1.28 eV, Figure S17i). This indicates that the H₂O generated from the reactions or added in the initial gas mixture may be preadsorbed at the catalyst surface and reduce the CH₃OH adsorption energy at its most stable site, which in a way promotes the desorption of CH₃OH. This agrees with our experimental results that H₂O addition increases the CH₃OH selectivity. However, it should also be noted that the excess

Table 1. Comparison of E_{ad} of CH_3OH over the $\text{Cu}_{13}/\gamma\text{-Al}_2\text{O}_3$ Surface under Different H_2O Preadsorption Conditions

H_2O number	H_2O adsorption site	CH_3OH adsorption site	CH_3OH adsorption energy (eV)
0		$\text{Cu}_{13}/\gamma\text{-Al}_2\text{O}_3$ interface	−1.45
0		Cu_{13} cluster	−0.84
0		$\gamma\text{-Al}_2\text{O}_3$ slab	−1.34
1	$\text{Cu}_{13}/\gamma\text{-Al}_2\text{O}_3$ interface	$\text{Cu}_{13}/\gamma\text{-Al}_2\text{O}_3$ interface	−1.23
1	$\text{Cu}_{13}/\gamma\text{-Al}_2\text{O}_3$ interface	Cu_{13} cluster	−0.80
1	$\text{Cu}_{13}/\gamma\text{-Al}_2\text{O}_3$ interface	$\gamma\text{-Al}_2\text{O}_3$ slab	−1.25
2	$\text{Cu}_{13}/\gamma\text{-Al}_2\text{O}_3$ interface	$\text{Cu}_{13}/\gamma\text{-Al}_2\text{O}_3$ interface	−1.17
2	$\text{Cu}_{13}/\gamma\text{-Al}_2\text{O}_3$ interface	Cu_{13} cluster	−0.74
2	$\text{Cu}_{13}/\gamma\text{-Al}_2\text{O}_3$ interface	$\gamma\text{-Al}_2\text{O}_3$ slab	−1.28

addition of H_2O could inhibit CH_3OH production, as shown in Figure 2b, and this also attributes to the competitive adsorption of the active sites, which negatively impact the hydrogenation of CO_2 and the adsorption of important intermediates.^{73,75,76}

3.8. Final Consideration. Overall, the $\text{Cu}/\gamma\text{-Al}_2\text{O}_3$ catalyst shows a good performance in plasma-catalytic CO_2 hydrogenation to CH_3OH . Our DFT simulations reveal that this is attributed to the high catalytic activity of the Cu atoms and the metal–support interaction. The interfacial site on $\text{Cu}_{13}/\gamma\text{-Al}_2\text{O}_3$ is considered to be bifunctional. First, it can effectively activate the CO_2 molecules. In addition, the intermediates in the CH_3OH synthesis process can be strongly adsorbed at this site, avoiding their desorption. CH_3OH can be generated through both RWGS and formate paths, while the CH_4 formation path is reduced due to its high activation barriers.

A thermal catalysis study showed that a 2–4 mm Cu cluster supported on $\gamma\text{-Al}_2\text{O}_3$ can catalyze the hydrogenation of CO_2 to CH_3OH , accompanied by the generation of CO and dimethyl ether (DME).⁶² Their DFT results also prove that the interface between the Cu cluster and the Al_2O_3 slab is the active site. DME and CO are produced by further dehydrogenation of CH_3OH and decomposition of surface species, respectively. Although we applied a similar $\text{Cu}/\gamma\text{-Al}_2\text{O}_3$ catalyst in plasma catalysis, DME did not show up in our experiments. This could be attributed to the synergistic effect between the plasma and catalyst, where the plasma species can accumulate on the catalyst surface and promote the CH_3OH desorption.⁷⁰ Besides, the adsorption of CH_3OH in our system is relatively weak due to the H_2O competitive adsorption so that desorption is easier than further dehydrogenation. Moreover, according to the analysis by Lam et al., competitive RWGS reactions could negatively impact the CH_3OH synthesis to reduce its yield and selectivity.⁶³ However, in plasma catalysis, the CO species generated in the plasma or at the catalyst surface may further participate in the surface reactions via the E–R mechanism and promote the selectivity toward CH_3OH .²⁷

In addition, complicated interactions can take place between the plasma and catalyst. Due to polarization effects, the $\text{Cu}/\gamma\text{-Al}_2\text{O}_3$ packing can effectively enhance the electric field inside the plasma, which leads to a more intense plasma and a higher

density of plasma species.^{77,78} Hence, these plasma species can participate in the CO_2 hydrogenation process via E–R reactions to reduce the reaction barriers and promote the generation of key intermediates in the catalytic reactions. Therefore, the plasma species can change the elementary reactions and tune the reaction pathways.

Furthermore, the plasma effects are not limited to E–R reactions. The electric field enhancement, as well as surface charging, may enhance the adsorption of CO_2 and promote its activation over the catalyst surface.^{79,80} In addition, the preadsorbed species on the catalyst surface or vibrational excited species in plasma catalysis can influence the surface reactions and hydrogenation process.^{45,81} These effects are not yet accounted for in our DFT calculations but may also be important to comprehensively understand the complete picture of plasma catalysis. Future studies should therefore include more detailed DFT calculations and in situ experiments.

4. CONCLUSIONS

We studied plasma-catalytic CO_2 hydrogenation to CH_3OH over a $\gamma\text{-Al}_2\text{O}_3$ supported Cu cluster catalyst, both experimentally and by DFT calculations to reveal the underlying mechanisms, with a special focus on the role of the plasma species via E–R mechanisms. The presence of the plasma allowed us to achieve a CO_2 conversion of 10% with a maximum CH_3OH selectivity of 65%, while no CO_2 conversion took place without the plasma under these conditions (room temperature and atmosphere pressure). Furthermore, the undesired CH_4 yield was reduced to below 2%. In addition, the energy efficiency was improved by more than a factor of 20 when combining the plasma and the $\text{Cu}/\gamma\text{-Al}_2\text{O}_3$ catalyst, as compared to plasma-only, indicating the key role of the active metal (Cu cluster) for efficiently producing CH_3OH . Our DFT results revealed that the interfacial site of $\text{Cu}_{13}/\gamma\text{-Al}_2\text{O}_3$ hosts multiple active sites for both the CO_2 activation and the hydrogenation. The reactive species generated in the plasma region could shift the barriers from the surface to the gas phase, thus reducing or eliminating the reaction barrier via the E–R mechanism, which makes the reaction take place under atmospheric conditions. Besides, H_2O competitive adsorption on the catalyst surface could promote the desorption of CH_3OH , thus increasing its selectivity. This study provides new insights into plasma-catalytic CO_2 hydrogenation to CH_3OH and may also have potential applications in other (plasma-)catalytic research, especially for SMC catalysts.

■ ASSOCIATED CONTENT

Supporting Information

The Supporting Information is available free of charge at <https://pubs.acs.org/doi/10.1021/acscatal.1c04678>.

More experimental details, choice of the supported cluster model, and computational details (PDF)

■ AUTHOR INFORMATION

Corresponding Authors

Yanhui Yi – State Key Laboratory of Fine Chemicals, School of Chemical Engineering, Dalian University of Technology, Dalian 116024, P. R. China; orcid.org/0000-0002-5869-9382; Email: yiyanhui@dlut.edu.cn

Xiaoxing Zhang – School of Electrical and Electronic Engineering, Hubei University of Technology, Wuhan 430068, China; Email: xiaoxing.zhang@outlook.com

Authors

Zhaolun Cui – School of Electric Power Engineering, South China University of Technology, Guangzhou 510630, China; Research Group PLASMAN, Department of Chemistry, University of Antwerp, Wilrijk-Antwerp BE-2610, Belgium

Shengyan Meng – State Key Laboratory of Fine Chemicals, School of Chemical Engineering, Dalian University of Technology, Dalian 116024, P. R. China

Amin Jafarzadeh – Research Group PLASMAN, Department of Chemistry, University of Antwerp, Wilrijk-Antwerp BE-2610, Belgium; orcid.org/0000-0002-1638-6222

Shangkun Li – Research Group PLASMAN, Department of Chemistry, University of Antwerp, Wilrijk-Antwerp BE-2610, Belgium; State Key Laboratory of Fine Chemicals, School of Chemical Engineering, Dalian University of Technology, Dalian 116024, P. R. China

Erik Cornelis Neyts – Research Group PLASMAN, Department of Chemistry, University of Antwerp, Wilrijk-Antwerp BE-2610, Belgium; orcid.org/0000-0002-3360-3196

Yanpeng Hao – School of Electric Power Engineering, South China University of Technology, Guangzhou 510630, China

Licheng Li – School of Electric Power Engineering, South China University of Technology, Guangzhou 510630, China

Xinkui Wang – State Key Laboratory of Fine Chemicals, School of Chemical Engineering, Dalian University of Technology, Dalian 116024, P. R. China

Annemie Bogaerts – Research Group PLASMAN, Department of Chemistry, University of Antwerp, Wilrijk-Antwerp BE-2610, Belgium; orcid.org/0000-0001-9875-6460

Complete contact information is available at:
<https://pubs.acs.org/10.1021/acscatal.1c04678>

Author Contributions

Z.C. and S.M. contributed equally to this paper. The manuscript was written through contributions of all authors. All authors have given approval to the final version of the manuscript.

Notes

The authors declare no competing financial interest.

ACKNOWLEDGMENTS

This research was funded by the National Natural Science Foundation of China (21503032 and 21978032) and the European Research Council (ERC) under the European Union's Horizon 2020 Research and Innovation Programme (ERC Synergy Grant 810182 SCOPE). The computational resources and services used in this work were provided by the HPC core facility CalcUA of the Universiteit Antwerpen and VSC (Flemish Supercomputer Center), funded by the Research Foundation—Flanders (FWO) and the Flemish Government.

REFERENCES

- (1) Bao, J.; Yang, G.; Yoneyama, Y.; Tsubaki, N. Significant Advances in C1 Catalysis: Highly Efficient Catalysts and Catalytic Reactions. *ACS Catal.* **2019**, *9*, 3026–3053.
- (2) Snoeckx, R.; Bogaerts, A. Plasma Technology-A Novel Solution for CO₂ Conversion? *Chem. Soc. Rev.* **2017**, *46*, 5805–5863.
- (3) Jiang, X.; Nie, X.; Guo, X.; Song, C.; Chen, J. G. Recent Advances in Carbon Dioxide Hydrogenation to Methanol via Heterogeneous Catalysis. *Chem. Rev.* **2020**, *120*, 7984–8034.
- (4) Zhong, J.; Yang, X.; Wu, Z.; Liang, B.; Huang, Y.; Zhang, T. State of The Art and Perspectives in Heterogeneous Catalysis of CO₂ Hydrogenation to Methanol. *Chem. Soc. Rev.* **2020**, *49*, 1385–1413.
- (5) Behrens, M.; Studt, F.; Kasatkin, I.; Kühl, S.; Hävecker, M.; Abild-Pedersen, F.; Zander, S.; Girsdiess, F.; Kurr, P.; Knief, B.-L.; Tovar, M.; Fischer, R. W.; Nørskov, J. K.; Schlögl, R. The Active Site of Methanol Synthesis over Cu/ZnO/Al₂O₃ Industrial Catalysts. *Science* **2012**, *336*, 893–897.
- (6) Graciani, J.; Mudiyanse, K.; Xu, F.; Baber, A. E.; Evans, J.; Senanayake, S. D.; Stacchiola, D. J.; Liu, P.; Hrbek, J.; Sanz, J. F.; Rodriguez, J. A. Highly Active Copper-Ceria and Copper-Ceria-Titania Catalysts for Methanol Synthesis from CO₂. *Science* **2014**, *345*, 546–550.
- (7) Kim, J.; Sarma, B. B.; Andrés, E.; Pfänder, N.; Concepción, P.; Prieto, G. Surface Lewis Acidity of Periphery Oxide Species as A General Kinetic Descriptor for CO₂ Hydrogenation to Methanol on Supported Copper Nanoparticles. *ACS Catal.* **2019**, *9*, 10409–10417.
- (8) Chen, S.; Zhang, J.; Song, F.; Zhang, Q.; Yang, G.; Zhang, M.; Wang, X.; Xie, H.; Tan, Y. Induced High Selectivity Methanol Formation During CO₂ Hydrogenation Over A CuBr₂-modified CuZnZr Catalyst. *J. Catal.* **2020**, *389*, 47–59.
- (9) Wu, C.; Lin, L.; Liu, J.; Zhang, J.; Zhang, F.; Zhou, T.; Rui, N.; Yao, S.; Deng, Y.; Yang, F.; Xu, W.; Luo, J.; Zhao, Y.; Yan, B.; Wen, X.-D.; Rodriguez, J. A.; Ma, D. Inverse ZrO₂/Cu as A Highly Efficient Methanol Synthesis Catalyst from CO₂ Hydrogenation. *Nat. Commun.* **2020**, *11*, 5767–5776.
- (10) Tada, S.; Otsuka, F.; Fujiwara, K.; Moularas, C.; Deligiannakis, Y.; Kinoshita, Y.; Uchida, S.; Honma, T.; Nishijima, M.; Kikuchi, R. Development of CO₂-to-Methanol Hydrogenation Catalyst by Focusing on the Coordination Structure of the Cu Species in Spinel-Type Oxide Mg_{1-x}Cu_xAl₂O₄. *ACS Catal.* **2020**, *10*, 15186–15194.
- (11) Zabilskiy, M.; Sushkevich, V. L.; Palagin, D.; Newton, M. A.; Krumeich, F.; van Bokhoven, J. A. The Unique Interplay Between Copper and Zinc During Catalytic Carbon Dioxide Hydrogenation to Methanol. *Nat. Commun.* **2020**, *11*, 2409.
- (12) Cui, X.; Yan, W.; Yang, H.; Shi, Y.; Xue, Y.; Zhang, H.; Niu, Y.; Fan, W.; Deng, T. Preserving the Active Cu-ZnO Interface for Selective Hydrogenation of CO₂ to Dimethyl Ether and Methanol. *ACS Sustain. Chem. Eng.* **2021**, *9*, 2661–2672.
- (13) Kattel, S.; Ramirez, P. J.; Chen, J. G.; Rodriguez, J. A.; Liu, P. CATALYSIS Active Sites for CO₂ hydrogenation to Methanol on Cu/ZnO Catalysts. *Science* **2017**, *355*, 1296.
- (14) Dong, C.; Li, Y.; Cheng, D.; Zhang, M.; Liu, J.; Wang, Y.-G.; Xiao, D.; Ma, D. Supported Metal Clusters: Fabrication and Application in Heterogeneous Catalysis. *ACS Catal.* **2020**, *10*, 11011–11045.
- (15) Liu, C.; Yang, B.; Tyo, E.; Seifert, S.; DeBartolo, J.; von Issendorff, B.; Zapol, P.; Vajda, S.; Curtiss, L. A. Carbon Dioxide Conversion to Methanol over Size-Selected Cu₄ Clusters at Low Pressures. *J. Am. Chem. Soc.* **2015**, *137*, 8676–8679.
- (16) Wang, L.; Yi, Y.; Guo, H.; Tu, X. Atmospheric Pressure and Room Temperature Synthesis of Methanol through Plasma-Catalytic Hydrogenation of CO₂. *ACS Catal.* **2018**, *8*, 90–100.
- (17) Wang, Z.; Zhang, Y.; Neyts, E. C.; Cao, X.; Zhang, X.; Jang, B. W.-L.; Liu, C.-j. Catalyst Preparation with Plasmas: How Does It Work? *ACS Catal.* **2018**, *8*, 2093–2110.
- (18) Neyts, E. C.; Ostrikov, K.; Sunkara, M. K.; Bogaerts, A. Plasma Catalysis: Synergistic Effects at the Nanoscale. *Chem. Rev.* **2015**, *115*, 13408–13446.
- (19) Engelmann, Y.; van 't Veer, K.; Gorbanev, Y.; Neyts, E. C.; Schneider, W. F.; Bogaerts, A. Plasma Catalysis for Ammonia Synthesis: A Microkinetic Modeling Study on the Contributions of

- Eley–Rideal Reactions. *ACS Sustain. Chem. Eng.* **2021**, *9*, 13151–13163.
- (20) Iliuta, I.; Larachi, F. Enhanced Methanol Synthesis Process via an Integrated Process Involving CO₂ Hydrogenation under Plasma Conditions. *Ind. Eng. Chem. Res.* **2020**, *59*, 6815–6827.
- (21) Wang, L.; Yi, Y.; Wu, C.; Guo, H.; Tu, X. One-Step Reforming of CO₂ and CH₄ into High-Value Liquid Chemicals and Fuels at Room Temperature by Plasma-Driven Catalysis. *Angew. Chem., Int. Ed.* **2017**, *56*, 13679–13683.
- (22) Wang, X.; Gao, Y.; Zhang, S.; Sun, H.; Li, J.; Shao, T. Nanosecond Pulsed Plasma Assisted Dry Reforming of CH₄: The Effect of Plasma Operating Parameters. *Appl. Energy* **2019**, *243*, 132–144.
- (23) Chen, H.; Goodarzi, F.; Mu, Y.; Chansai, S.; Mielby, J. J.; Mao, B.; Sooknoi, T.; Hardacre, C.; Kegnaes, S.; Fan, X. Effect of Metal Dispersion and Support Structure of Ni/silicalite-1 Catalysts on Non-Thermal Plasma (NTP) Activated CO₂ Hydrogenation. *Appl. Catal., B* **2020**, *272*, 119013.
- (24) Ronda-Lloret, M.; Wang, Y.; Oulego, P.; Rothenberg, G.; Tu, X.; Shiju, N. R. CO₂ Hydrogenation at Atmospheric Pressure and Low Temperature Using Plasma-Enhanced Catalysis over Supported Cobalt Oxide Catalysts. *ACS Sustain. Chem. Eng.* **2020**, *8*, 17397–17407.
- (25) Xu, S.; Chansai, S.; Shao, Y.; Xu, S.; Wang, Y.-c.; Haigh, S.; Mu, Y.; Jiao, Y.; Stere, C. E.; Chen, H.; Fan, X.; Hardacre, C. Mechanistic Study of Non-Thermal Plasma Assisted CO₂ Hydrogenation over Ru Supported on MgAl Layered Double Hydroxide. *Appl. Catal., B* **2020**, *268*, 118752.
- (26) Bogaerts, A.; Tu, X.; Whitehead, J. C.; Centi, G.; Lefferts, L.; Guaitella, O.; Azzolina-Jury, F.; Kim, H.-H.; Murphy, A. B.; Schneider, W. F.; Nozaki, T.; Hicks, J. C.; Rousseau, A.; Thevenet, F.; Khacef, A.; Carreon, M. The 2020 Plasma Catalysis Roadmap. *J. Phys. D: Appl. Phys.* **2020**, *53*, 443001–443052.
- (27) Michiels, R.; Engelmann, Y.; Bogaerts, A. Plasma Catalysis for CO₂ Hydrogenation: Unlocking New Pathways toward CH₃OH. *J. Phys. Chem. C* **2020**, *124*, 25859–25872.
- (28) Mu, Y.; Xu, S.; Shao, Y.; Chen, H.; Hardacre, C.; Fan, X. Kinetic Study of Nonthermal Plasma Activated Catalytic CO₂ Hydrogenation over Ni Supported on Silica Catalyst. *Ind. Eng. Chem. Res.* **2020**, *59*, 9478–9487.
- (29) Ye, J.; Liu, C.-j.; Mei, D.; Ge, Q. Methanol Synthesis from CO₂ Hydrogenation over a Pd₄/In₂O₃ Model Catalyst: A Combined DFT and Kinetic Study. *J. Catal.* **2014**, *317*, 44–53.
- (30) Dang, S.; Qin, B.; Yang, Y.; Wang, H.; Cai, J.; Han, Y.; Li, S.; Gao, P.; Sun, Y. Rationally Designed Indium Oxide Catalysts for CO₂ Hydrogenation to Methanol with High Activity and Selectivity. *Sci. Adv.* **2020**, *6*, No. eaaz2060.
- (31) Grabow, L. C.; Mavrikakis, M. Mechanism of Methanol Synthesis on Cu through CO₂ and CO Hydrogenation. *ACS Catal.* **2011**, *1*, 365–384.
- (32) Studt, F.; Behrens, M.; Kunkes, E. L.; Thomas, N.; Zander, S.; Tarasov, A.; Schumann, J.; Frei, E.; Varley, J. B.; Abild-Pedersen, F.; Nørskov, J. K.; Schlögl, R. The Mechanism of CO and CO₂ Hydrogenation to Methanol over Cu-Based Catalysts. *ChemCatChem* **2015**, *7*, 1105–1111.
- (33) Zhao, Y.-F.; Yang, Y.; Mims, C.; Peden, C. H. F.; Li, J.; Mei, D. Insight into Methanol Synthesis from CO₂ Hydrogenation on Cu(111): Complex Reaction Network and the Effects of H₂O. *J. Catal.* **2011**, *281*, 199–211.
- (34) Yang, Y.; Evans, J.; Rodriguez, J. A.; White, M. G.; Liu, P. Fundamental Studies of Methanol Synthesis from CO₂ Hydrogenation on Cu(111), Cu Clusters, and Cu/ZnO (0001). *Phys. Chem. Chem. Phys.* **2010**, *12*, 9909–9917.
- (35) Hutter, J.; Iannuzzi, M.; Schiffmann, F.; VandeVondele, J. CP2K: Atomistic Simulations of Condensed Matter Systems. *Wiley Interdiscip. Rev. Comput. Mol. Sci.* **2014**, *4*, 15–25.
- (36) VandeVondele, J.; Krack, M.; Mohamed, F.; Parrinello, M.; Chassaing, T.; Hutter, J. QUICKSTEP: Fast and Accurate Density Functional Calculations Using a Mixed Gaussian and Plane Waves Approach. *Comput. Phys. Commun.* **2005**, *167*, 103–128.
- (37) VandeVondele, J.; Hutter, J. Gaussian Basis Sets for Accurate Calculations on Molecular Systems in Gas and Condensed Phases. *J. Chem. Phys.* **2007**, *127*, 114105.
- (38) Goedecker, S.; Teter, M.; Hutter, J. Separable Dual-Space Gaussian Pseudopotentials. *Phys. Rev. B: Condens. Matter Mater. Phys.* **1996**, *54*, 1703–1710.
- (39) Krack, M. Pseudopotentials for H to Kr Optimized for Gradient-Corrected Exchange-Correlation Functionals. *Theor. Chem. Acc.* **2005**, *114*, 145–152.
- (40) Perdew, J. P.; Burke, K.; Ernzerhof, M. Generalized Gradient Approximation Made Simple. *Phys. Rev. Lett.* **1996**, *77*, 3865–3868.
- (41) Grimme, S.; Antony, J.; Ehrlich, S.; Krieg, H. A Consistent and Accurate Ab Initio Parametrization of Density Functional Dispersion Correction (DFT-D) for the 94 Elements H–Pu. *J. Chem. Phys.* **2010**, *132*, 154104.
- (42) Head, J. D.; Zerner, M. C. A Broyden–Fletcher–Goldfarb–Shanno Optimization Procedure for Molecular Geometries. *Chem. Phys. Lett.* **1985**, *122*, 264–270.
- (43) Henkelman, G.; Arnaldsson, A.; Jónsson, H. A Fast and Robust Algorithm for Bader Decomposition of Charge Density. *Comput. Mater. Sci.* **2006**, *36*, 354–360.
- (44) Henkelman, G.; Uberuaga, B. P.; Jónsson, H. A Climbing Image Nudged Elastic Band Method for Finding Saddle Points and Minimum Energy Paths. *J. Chem. Phys.* **2000**, *113*, 9901–9904.
- (45) Digne, M.; Sautet, P.; Raybaud, P.; Euzen, P.; Toulhoat, H. Use of DFT to Achieve a Rational Understanding of Acid-Basic Properties of γ -Alumina Surfaces. *J. Catal.* **2004**, *226*, 54–68.
- (46) Silaghi, M.-C.; Comas-Vives, A.; Copéret, C. CO₂ Activation on Ni/ γ -Al₂O₃ Catalysts by First-Principles Calculations: From Ideal Surfaces to Supported Nanoparticles. *ACS Catal.* **2016**, *6*, 4501–4505.
- (47) Wischert, R.; Laurent, P.; Copéret, C.; Delbecq, F.; Sautet, P. γ -Alumina: The Essential and Unexpected Role of Water for the Structure, Stability, and Reactivity of “Defect” Sites. *J. Am. Chem. Soc.* **2012**, *134*, 14430–14449.
- (48) Shirazi, M.; Neyts, E. C.; Bogaerts, A. DFT study of Ni-Catalyzed Plasma Dry Reforming of Methane. *Appl. Catal., B* **2017**, *205*, 605–614.
- (49) Bal, K. M.; Huygh, S.; Bogaerts, A.; Neyts, E. C. Effect of Plasma-Induced Surface Charging on Catalytic Processes: Application to CO₂ Activation. *Plasma Sources Sci. Technol.* **2018**, *27*, 024001.
- (50) Gutterød, E. S.; Pulumati, S. H.; Kaur, G.; Lazzarini, A.; Solemsli, B. G.; Gunnæs, A. E.; Ahoba-Sam, C.; Kalyva, M. E.; Sannes, J. A.; Svelle, S.; Skúlason, E.; Nova, A.; Olsbye, U. Influence of Defects and H₂O on the Hydrogenation of CO₂ to Methanol over Pt Nanoparticles in UiO-67 Metal-Organic Framework. *J. Am. Chem. Soc.* **2020**, *142*, 17105–17118.
- (51) Wang, Y.; Gao, W.; Li, K.; Zheng, Y.; Xie, Z.; Na, W.; Chen, J. G.; Wang, H. Strong Evidence of the Role of H₂O in Affecting Methanol Selectivity from CO₂ Hydrogenation over Cu–ZnO–ZrO₂. *Chem* **2020**, *6*, 419–430.
- (52) Jiang, X.; Nie, X.; Gong, Y.; Moran, C. M.; Wang, J.; Zhu, J.; Chang, H.; Guo, X.; Walton, K. S.; Song, C. A Combined Experimental and DFT Study of H₂O Effect on In₂O₃/ZrO₂ Catalyst for CO₂ Hydrogenation to Methanol. *J. Catal.* **2020**, *383*, 283–296.
- (53) Gorbanev, Y.; Vervloessem, E.; Nikiforov, A.; Bogaerts, A. Nitrogen Fixation with Water Vapor by Nonequilibrium Plasma: Toward Sustainable Ammonia Production. *ACS Sustain. Chem. Eng.* **2020**, *8*, 2996–3004.
- (54) Snoeckx, R.; Ozkan, A.; Reniers, F.; Bogaerts, A. The Quest for Value-Added Products from Carbon Dioxide and Water in a Dielectric Barrier Discharge: A Chemical Kinetics Study. *ChemSusChem* **2017**, *10*, 409–424.
- (55) Zhao, B.; Liu, Y.; Zhu, Z.; Guo, H.; Ma, X. Highly Selective Conversion of CO₂ into Ethanol on Cu/ZnO/Al₂O₃ Catalyst with the Assistance of Plasma. *J. CO₂ Util.* **2018**, *24*, 34–39.

- (56) Zambrano, G.; Riascos, H.; Prieto, P.; Restrepo, E.; Devia, A.; Rincón, C. Optical Emission Spectroscopy Study of R.f. Magnetron Sputtering Discharge Used for Multilayers Thin Film Deposition. *Surf. Coat. Technol.* **2003**, *172*, 144–149.
- (57) Kholodkov, A. V.; Golant, K. M.; Nikolin, I. V. Nano-scale Compositional Lamination of Doped Silica Glass Deposited in Surface Discharge Plasma of SPCVD Technology. *Microelectron. Eng.* **2003**, *69*, 365–372.
- (58) Czerwicz, T.; Gavillet, J.; Belmonte, T.; Michel, H.; Ricard, A. Determination of O Atom Density in Ar-O₂ and Ar-O₂-H₂ Flowing Microwave Discharges. *Surf. Coat. Technol.* **1998**, *98*, 1411–1415.
- (59) Granier, A.; Vervloet, M.; Aumaille, K.; Valle, C. Optical Emission Spectra of TEOS and HMDSO Derived Plasmas Used for Thin Film Deposition. *Plasma Sources Sci. Technol.* **2003**, *12*, 89–96.
- (60) Yi, Y.; Wang, X.; Jafarzadeh, A.; Wang, L.; Liu, P.; He, B.; Yan, J.; Zhang, R.; Zhang, H.; Liu, X.; Guo, H.; Neyts, E. C.; Bogaerts, A. Plasma-Catalytic Ammonia Reforming of Methane over Cu-Based Catalysts for the Production of HCN and H₂ at Reduced Temperature. *ACS Catal.* **2021**, *11*, 1765–1773.
- (61) Cai, F.; Zhu, W.; Xiao, G. Promoting Effect of Zirconium Oxide on Cu-Al₂O₃ Catalyst for the Hydrogenolysis of Glycerol to 1, 2-Propanediol. *Catal. Sci. Technol.* **2016**, *6*, 4889–4900.
- (62) Yoshida, H.; Hirakawa, T.; Oyama, H.; Nakashima, R.; Hinokuma, S.; Machida, M. Effect of Thermal Aging on Local Structure and Three-Way Catalysis of Cu/Al₂O₃. *J. Phys. Chem. C* **2019**, *123*, 10469–10476.
- (63) Lam, E.; Corral-Pérez, J. J.; Larmier, K.; Noh, G.; Wolf, P.; Comas-Vives, A.; Urakawa, A.; Copéret, C. CO₂ Hydrogenation on Cu/Al₂O₃: Role of Metal/Support Interface in Driving Activity and Selectivity of a Bifunctional Catalyst. *Angew. Chem., Int. Ed.* **2019**, *58*, 13989–13996.
- (64) Sun, Q.; Liu, C.-W.; Pan, W.; Zhu, Q.-M.; Deng, J.-F. In Situ IR Studies on the Mechanism of Methanol Synthesis over an Ultrafine Cu/ZnO/Al₂O₃ Catalyst. *Appl. Catal., A* **1998**, *171*, 301–308.
- (65) Edwards, J. F.; Schrader, G. L. In Situ Fourier Transform Infrared Study of Methanol Synthesis on Mixed Metal Oxide Catalysts. *J. Catal.* **1985**, *94*, 175–186.
- (66) Clarke, D. B.; Bell, A. T. An Infrared Study of Methanol Synthesis from CO₂ on Clean and Potassium-promoted Cu/SiO₂. *J. Catal.* **1995**, *154*, 314–328.
- (67) Kattel, S.; Liu, P.; Chen, J. G. Tuning Selectivity of CO₂ Hydrogenation Reactions at the Metal/Oxide Interface. *J. Am. Chem. Soc.* **2017**, *139*, 9739–9754.
- (68) Azzolina-Jury, F.; Thibault-Starzyk, F. Mechanism of Low Pressure Plasma-Assisted CO₂ Hydrogenation Over Ni-USY by Microsecond Time-resolved FTIR Spectroscopy. *Top. Catal.* **2017**, *60*, 1709–1721.
- (69) Xu, S.; Chansai, S.; Xu, S.; Stere, C. E.; Jiao, Y.; Yang, S.; Hardacre, C.; Fan, X. CO Poisoning of Ru Catalysts in CO₂ Hydrogenation under Thermal and Plasma Conditions: A Combined Kinetic and Diffuse Reflectance Infrared Fourier Transform Spectroscopy-Mass Spectrometry Study. *ACS Catal.* **2020**, *10*, 12828–12840.
- (70) De Bie, C.; van Dijk, J.; Bogaerts, A. CO₂ Hydrogenation in a Dielectric Barrier Discharge Plasma Revealed. *J. Phys. Chem. C* **2016**, *120*, 25210–25224.
- (71) Wang, G.; Morikawa, Y.; Matsumoto, T.; Nakamura, J. Why Is Formate Synthesis Insensitive to Copper Surface Structures? *J. Phys. Chem. B* **2006**, *110*, 9–11.
- (72) Mei, D.; Xu, L.; Henkelman, G. Dimer Saddle Point Searches to Determine the Reactivity of Formate on Cu(111). *J. Catal.* **2008**, *258*, 44–51.
- (73) Wang, Y.; Kattel, S.; Gao, W.; Li, K.; Liu, P.; Chen, J. G.; Wang, H. Exploring the Ternary Interactions in Cu-ZnO-ZrO₂ Catalysts for Efficient CO₂ Hydrogenation to Methanol. *Nat. Commun.* **2019**, *10*, 1166.
- (74) Lustemberg, P. G.; Palomino, R. M.; Gutiérrez, R. A.; Grinter, D. C.; Vorokhta, M.; Liu, Z.; Ramírez, P. J.; Matolín, V.; Ganduglia-Pirovano, M. V.; Senanayake, S. D.; Rodriguez, J. A. Direct Conversion of Methane to Methanol on Ni-Ceria Surfaces: Metal-Support Interactions and Water-Enabled Catalytic Conversion by Site Blocking. *J. Am. Chem. Soc.* **2018**, *140*, 7681–7687.
- (75) Kung, H. H. Deactivation of Methanol Synthesis Catalysts-A Review. *Catal. Today* **1992**, *11*, 443–453.
- (76) Saito, M.; Fujitani, T.; Takeuchi, M.; Watanabe, T. Development of Copper/Zinc Oxide-based Multicomponent Catalysts for Methanol Synthesis from Carbon Dioxide and Hydrogen. *Appl. Catal., A* **1996**, *138*, 311–318.
- (77) Butterworth, T.; Elder, R.; Allen, R. Effects of Particle Size on CO₂ Reduction and Discharge Characteristics in a Packed Bed Plasma Reactor. *Chem. Eng. J.* **2016**, *293*, 55–67.
- (78) Van Laer, K.; Bogaerts, A. Fluid Modelling of a Packed Bed Dielectric Barrier Discharge Plasma Reactor. *Plasma Sources Sci. Technol.* **2016**, *25*, 015002.
- (79) Jafarzadeh, A.; Bal, K. M.; Bogaerts, A.; Neyts, E. C. CO₂ Activation on TiO₂-Supported Cu₅ and Ni₅ Nanoclusters: Effect of Plasma-Induced Surface Charging. *J. Phys. Chem. C* **2019**, *123*, 6516–6525.
- (80) Jafarzadeh, A.; Bal, K. M.; Bogaerts, A.; Neyts, E. C. Activation of CO₂ on Copper Surfaces: The Synergy Between Electric Field, Surface Morphology, and Excess Electrons. *J. Phys. Chem. C* **2020**, *124*, 6747–6755.
- (81) Quan, J.; Muttaqien, F.; Kondo, T.; Kozarashi, T.; Mogi, T.; Imabayashi, T.; Hamamoto, Y.; Inagaki, K.; Hamada, I.; Morikawa, Y.; Nakamura, J. Vibration-driven Reaction of CO₂ on Cu Surfaces via Eley-Rideal-type Mechanism. *Nat. Chem.* **2019**, *11*, 722–729.

Recommended by ACS

On the Role of Hydroxyl Groups on Cu/Al₂O₃ in CO₂ Hydrogenation

Xiwen Song, Jinlong Gong, *et al.*

NOVEMBER 04, 2022
ACS CATALYSIS

READ 

Hydrogenation of Formate Species Using Atomic Hydrogen on a Cu(111) Model Catalyst

Kotaro Takeyasu, Junji Nakamura, *et al.*

JUNE 28, 2022
JOURNAL OF THE AMERICAN CHEMICAL SOCIETY

READ 

CO₂ Hydrogenation to Methanol over Inverse ZrO₂/Cu(111) Catalysts: The Fate of Methoxy under Dry and Wet Conditions

Ning Rui, José A. Rodriguez, *et al.*

AUGUST 18, 2022
THE JOURNAL OF PHYSICAL CHEMISTRY C

READ 

Selective Methane Oxidation to Methanol on ZnO/Cu₂O/Cu(111) Catalysts: Multiple Site-Dependent Behaviors

Erwei Huang, Ping Liu, *et al.*

NOVEMBER 04, 2021
JOURNAL OF THE AMERICAN CHEMICAL SOCIETY

READ 

Get More Suggestions >